

Mechanisms of electrical conductivity, quantum capacity and negative capacitance effects in InSe<PTHQ> nanohybrid

Fedir IVASHCHYSHYN^{1*}, Vitaliy MAKSYMCH², Dariusz CALUS¹, Myroslava KLAPCHUK²,
Glib BARYSHNIKOV³, Rostislav GALAGAN³, Valentina LITVIN³, Piotr CHABECKI¹,
and Ihor BORDUN^{1,2}

¹Czestochowa University of Technology, Al. Armii Krajowej 17, Czestochowa, 42-200, Poland,

²Lviv Polytechnic National University, Bandera Str. 12, Lviv, 79013, Ukraine

³Bohdan Khmelnytsky National University, blvd. Shevchnko 81, 18031, Cherkasy, Ukraine

Abstract. In this work, we present findings on the syntheses and study of properties of InSe<PTHQ> nanohybrid. The introduction of guest component in GaSe matrix leads to an increase in inhomogeneities, which is clearly confirmed by the strengthening of the low-frequency horizontal branch of Nyquist diagrams. A constant magnetic field counteracts this effect and changes the behavior of the impedance hodograph at low frequencies to the opposite. Illumination leads to a colossal increase in quantum capacitance, which is clearly demonstrated in the Nyquist diagram. For the synthesized InSe<PTHQ> nanohybrid the interesting behavior of the current-voltage characteristic is reported. As a result of studies of the synthesized InSe<PTHQ> nanohybrid the effect of “negative capacity” is observed, the magnitude of which can be controlled by the electric field. Based on the constructed impedance model and proposed N-barrier model, the physical mechanisms of the investigated processes are suggested.

Key words: InSe; intercalation; hierarchical structures; impedance spectroscopy; density of states; negative capacity.

1. INTRODUCTION

Modern development of nanotechnologies and nanodevices has brought to the forefront the task of creating new functional materials and nano systems based on them. Scientists are increasingly focused on hybrid inorganic/organic materials. The interest lies in the possibility of obtaining structures with a wide range of new, hitherto unknown properties. Significant success has been achieved in the direction of supramolecular chemistry [1–3], while only the first steps are being taken in the development of the physical basis for understanding the effects and phenomena associated with the supramolecular structure of substances.

Thanks to recent advances in fabrication of multilayered nanostructures, several kinds of heterostructure nanocomposite materials with a supramolecular guest component have been synthesized with highly anisotropic electronic properties which allow to realize quantum strengthening of sensory sensitivity to external physical fields [4] and the fundamental possibility to convert and accumulate electrical energy at the quantum level [5, 6].

The aim of the present paper is to describe a theoretical approach for the formation of intercalated heterostructures with

various geometry, composition, and level of hierarchical architecture. Electronic transport through a multilayer nanostructure is in effect a wave transmitting process of electrons [7]. The current through heterostructure can be represented with the transmission probability and the Fermi distribution function. We use Thomas–Fermi model where quantum mechanical part of the problem is described by a semiclassical approach, namely Thomas–Fermi approximation and the electrostatic part of the problem is described by the Poisson equation.

2. BASIC CONCEPT AND METHOD OF EXPERIMENT

An InSe single crystal was chosen as a semiconductor inorganic matrix with a pronounced layered structure, and polythiocyanatohydroquinone (PTHQ) was chosen as an organic component [8]. This organic compound is a polymer that can be represented as an amorphous mixture of linear polymer chains of different lengths. The real structure can be interpreted as a branched dendrimer-like composition. The experimental absorption spectrum consists of a single absorption band with a maximum at 315 nm and a wide unstructured absorption band in the region on the right side.

In our previous studies, it was found that InSe single crystals are easily subjected to electrochemical intercalation of s-, p- and d-elements, their co-intercalation [9]. Ferroelectrics as NaNO₂ are directly introduced into their structure from the melt [10]. However, organic cavitand PTHQ cannot be directly

*e-mail: fedirivashchyshyn@gmail.com

Manuscript submitted 2021-06-10, revised 2021-07-16, initially accepted for publication 2021-08-21, published in February 2022.

inserted into the van der Waals bond region of these crystal lattices due to geometric incompleteness. To overcome this obstacle, we used a three-stage scheme of intercalation crystal engineering (Fig. 1).

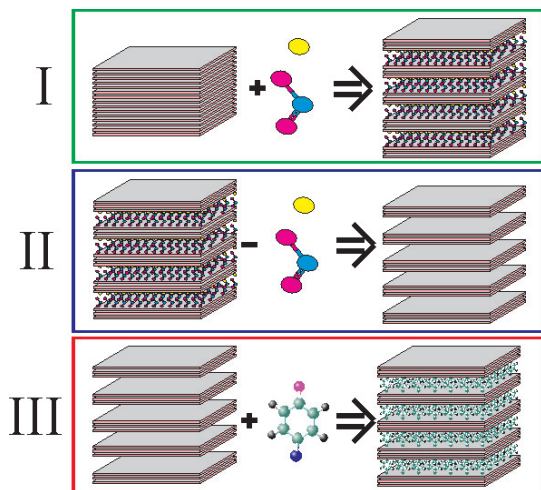


Fig. 1. Stages of formation of multilayer nanostructures GaSe<PTHQ>

In the first stage, sodium nitrite NaNO_2 is introduced into the initial matrix by direct exposure in its melt of GaSe and InSe semiconductor crystals at a temperature of 300°C and exposure duration of $5 \div 20$ minutes depending on the required degree of crystal lattice expansion. As a result of n -stage ordering, the distance between the individual layers increases several times.

The next step was deintercalation of sodium nitrite from the crystal by extracting it with distilled water it over a five-times 24-hour cycle and drying at $\sim 110^\circ\text{C}$ and reduced pressure ($10^{-1} \div 10^{-2}$ mm Hg). The deintercalated matrix has become suitable for the introduction of organic content due to significantly weakened van der Waals bonds and modified intracrystalline force fields. As a result, a double degree of matrix expansion was achieved in Se.

Therefore, in the third stage, intercalation formation of nanolayers PTHQ in an expanded crystal lattice was performed by direct exposure in the liquid-phase “guest” component of the obtained deintercalated matrices at room temperature for 24 hours.

Further the samples were dried at a temperature of $30 \div 40^\circ\text{C}$. After that, ohmic contacts were applied to both faces (perpendicular to the crystallographic axis C) of the obtained nanostructure.

Impedance measurements were performed using AUTOLAB measuring system (ECO CHEMIE, Netherlands) equipped with FRA-2 and GPES software in the direction of the crystallographic axis C (perpendicular to the layers) in the frequency range $10^{-3} \div 10^5$ Hz. Measurements were performed in a constant magnetic field (2.75 kOe) or under illumination (for the standard AM 1.5 G solar spectrum, the total available power is 982 W/m^2). A constant magnetic field intensity of 2.75 kOe and illumination was applied during the measurements along the measuring signal (perpendicular to the layers of the sin-

gle crystal). This geometry of measurements was chosen to collinear action of the constant magnetic field and the current of the measuring signal.

3. RESULTS AND DISCUSSION

To elucidate the nature of properties of nano hybrids, X-ray diffraction studies of the initial crystal matrix and matrix with twice degrees of expansion were performed. X-ray diffraction spectra were obtained on a diffractometer in $\text{CuK}\alpha$ radiation, monochromatized by reflection from the planes (200) of a single crystal LiF mounted on the primary beam, in a symmetrical version of $\theta-2\theta$ scanning. A series of maxima from the crystallographic planes (002), (004), (006), (008), (00 10), (00 12), (00 14), (00 16), (00 18) and (00 20) is observed on the diffractograms of the unexpanded, double- and triple-expanded InSe matrix. The obtained results make it possible to calculate the parameter from the unit cell of the indium selenide phase. For this purpose, the maximum profile (00 16) was analyzed, which is characterized by sufficient intensity and clear splitting of the doublet $\text{K}\alpha_{1,2}$. The maximum profile was approximated by superposition of Gaussian functions for each doublet component (Fig. 2). The parameter of unit cell c was determined exactly by the formula:

$$c = \frac{\lambda_{\text{K}\alpha 1}}{2 \cdot \sin(\vartheta_{\text{K}\alpha 1})} \cdot (h^2 + k^2 + l^2), \quad (1)$$

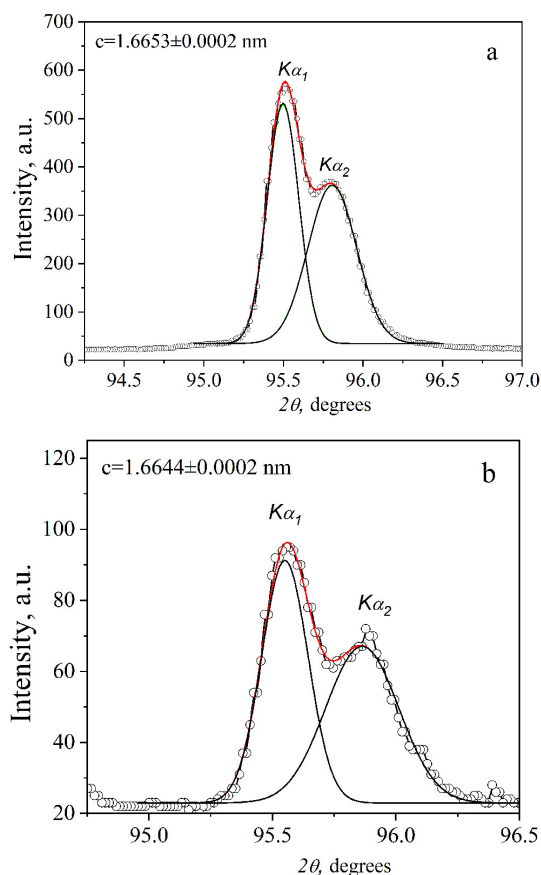


Fig. 2. X-ray diffraction pattern, maximum from the crystallographic plane (00 16) for InSe: a – not expanded matrix, b – twice expanded

where $\lambda_{K\alpha 1} = 0.15406 \text{ nm} \cdot 2\vartheta_{K\alpha 1}$ is the angular position of the component $K\alpha 1$ of the doublet, (h, k, l) are the Miller indices $h = k = 0, l = 4$. The increase in the degree of expansion of the crystal lattice along the crystallographic axis C is accompanied by a decrease in the corresponding lattice parameter compared to the original sample, which indicates a decrease in the interlayer distance in undeveloped packages InSe. In addition to shifting the angular position of the Bragg peak, there is also an increase in the half-width of the diffraction reflection curves compared to the original sample. The expansion of the reflection curves is proportional to the relative change in the interplanar distance, i.e., indicates the presence of fluctuations in the distance between the layers in single crystals. Therefore, we can say that as a result of the expansion of single crystals, an N -stage ordered structure is formed. It consists of identical packets (with slightly compressed interlayer distances compared to the original single crystal) which are separated by an extended area.

The next step was to study the impedance spectra of complex electrical conductivity.

Figure 3 shows the frequency dependences of the real component of the specific complex impedance ($\text{Re}Z(\omega)$) of the original extended matrix InSe and the intercalated nano hybrid InSe<PTHQ> measured under normal conditions, under the action of a constant magnetic field and under the illumination.

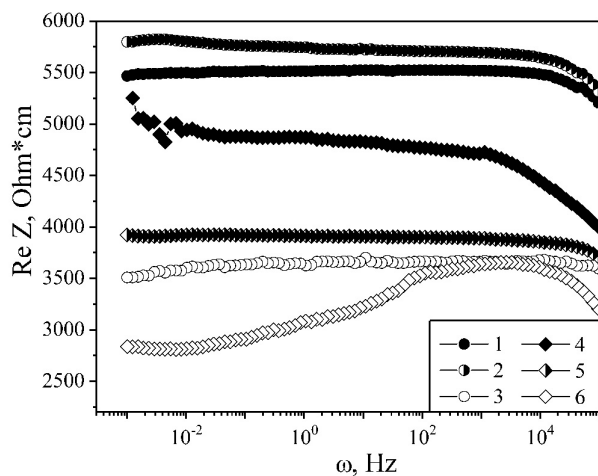


Fig. 3. Frequency dependences of the complex impedance perpendicular to the nanolayers of the extended matrix InSe (1–3) and nanostructure InSe<PTHQ> (4–6), measured in the dark (1, 4), in a constant magnetic field (2, 5) and under the illumination (3, 6)

First of all, it can be seen that the PTHQ intercalation leads to a decrease in $\text{Re}Z(\omega)$ and to a narrowing of the frequency-independent section of the hodograph. In the case of the original extended matrix, we have the usual picture [11], but for the intercalated nano hybrid InSe<PTHQ> the picture is radically different: there are oscillations of $\text{Re}Z(\omega)$ in the lowest frequency part of the spectrum and a significant increase in conductivity in the high frequency region starting from 10^3 Hz. The first phenomenon can be caused by the formation by intercalation of guest content of trap centers, which are able to

capture and hold current carriers over the time associated with the half-period of a sinusoidal signal when measuring the frequency spectra. The second phenomenon arises due to the increase in the contribution to the electrical conductivity of delocalized carriers against the background of the contribution of hopping conductivity to localized states near the Fermi level.

The next step was the impedance studies in the application of a constant magnetic field. For the original extended matrix, we observe a slight positive magnetoresistive effect. However, for the intercalated InSe<PTHQ> nano hybrid, the picture was quite the opposite: a much higher magnetoresistive effect was observed. It should be noted that the constant magnetic field completely eliminates the low-frequency oscillations of $\text{Re}Z(\omega)$ and the dependence takes on a linear character almost independently of the frequency in the entire frequency range. It is most likely that a constant magnetic field leads to a symmetrization of the distribution of impurity energy levels near the Fermi level, thus eliminating the contribution to the overall conductivity of the jump conductivity of nonequilibrium current carriers, which takes place under normal conditions.

Next, we studied the effect of lighting on the electrical properties of the test sample. The original crystal matrix is obviously photosensitive, so when illuminated, we expect to obtain a decrease in $\text{Re}Z(\omega)$ ($\rho_{\text{dark}}/\rho_{\text{light}} \approx 1.40$). The dependence curve $\text{Re}Z(\omega)$ has the same character as for the extended matrix measured under normal conditions. However, for the intercalated nano hybrid InSe<PTHQ> there is not only an increase in photosensitivity ($\rho_{\text{dark}}/\rho_{\text{light}} \approx 1.78$), but, more interestingly, the anomalous behavior (increase with frequency) of the dependence of $\text{Re}Z(\omega)$ (curve 6, Fig. 1). As can be seen from this figure, white light suppressing the frequency independence of $\text{Re}Z(\omega)$, causes its dispersion. Irradiation of the nanostructure with visible light leads to the generation of nonequilibrium carriers, which filling the bottom of the conduction band create conditions for the visualization of quantum capacity C_Q due to either deformation of the applied field 2D-electron gas, or finite tunneling times [12]. As a result, the conductivity of nonequilibrium carriers should decrease with increasing frequency, which is observed.

A clear confirmation of the above is the Nyquist diagrams, which are presented in Fig. 4. One can see for the original extended matrix InSe measured under normal conditions, a classical picture is observed, and the incompleteness of the arc of the impedance hodograph in the high frequency region limited to scanning the frequency range up to 1 MHz. This behavior of the complex resistance can be simulated by connecting a resistor and a capacitor in parallel (parallel RC link).

The action of a constant magnetic field does not make a significant change in the high-frequency behavior of the complex resistance, but it should be noted the difference of low-frequency region: horizontal branch directed toward the growth of the real part of the complex resistance is visualized.

This phenomenon is associated with the spatial inhomogeneity of electrical conductivity introduced by a constant magnetic field, which in the simulation can be represented by the BCPE element [13, 14], which reflects the current in a spatially bounded region with complex electrical conductivity. White

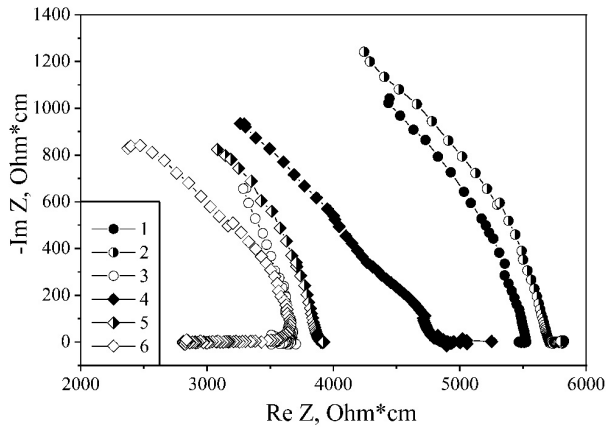


Fig. 4. Nyquist diagrams of the extended matrix InSe (1–3) and nanostructures InSe<PTHQ> (4–6), measured in the dark (1, 4), at the action of a constant magnetic field (2, 5) and under illumination (3, 6)

light also dramatically changes the low-frequency behavior of the impedance hodograph. The horizontal branch directed towards the reduction of the real part of the complex impedance can be represented by a quantum Lury capacitance, which is connected in parallel to the series RC link.

The introduction of guest content leads to an increase in inhomogeneities, which is clearly confirmed by the strengthening of the low-frequency horizontal branch of the impedance hodograph, which acquires a pronounced character. The constant magnetic field neutralizes this effect, which confirms the above assumption of the mechanism of this phenomenon. Instead, illumination leads to a colossal increase in quantum capacity, which is clearly demonstrated in the Nyquist diagram.

Analyzing the above results, their significant value from a practical point of view should be noted, because in this nanohybridized structure it was possible to obtain photoinduced quantum capacity, which allows in such a system to convert solar energy and accumulate it at the quantum level. This in turn opens new opportunities in the use of solar energy and autonomous power supplies.

Another confirmation of the unusual behavior of the intercalated nanohybrid in the field of the light wave is the appearance of the volt-ampere characteristic presented in Fig. 5. To clarify the nature of this phenomenon, consider the following model.

In [15], the synthesized nanohybrid as an N -barrier structure was presented, the structure of which is schematically shown in Fig. 6.

It shows the extended van der Waals region occupied by PTHQ polymer (Fig. 6(I)), denoted by 1, and the semiconductor by 2. Given idealization of real heterostructure with stuck ordered domains allows us to make analytical progress and yield more insight. We assume that the polymer carriers delocalized by light – holes – are positioned on the central symmetry axis of region 1. It is obvious that the polymer layers of the p-type will play the role of potential barriers for n-type electrons of InSe. The nanoscale of the matrix layer is considered by the fact that the double shielding radius of Thomas–Fermi is proportional to the width b . This in turn will lead to the fact that

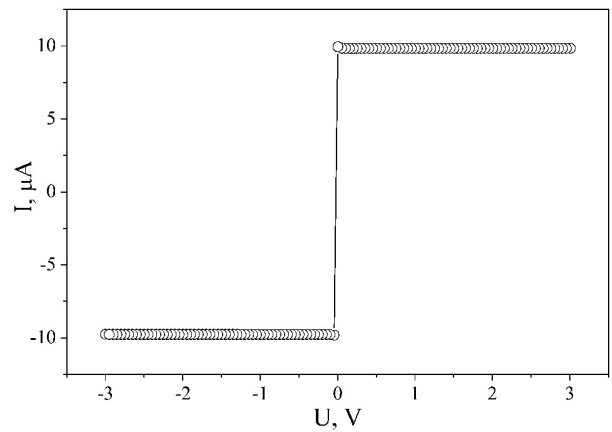


Fig. 5. I–V characteristic of InSe<PTHQ> nanostructure measured under illumination

the energy relief for the motion of the electron along the C axis will have the form shown in Fig. 6(II).

The classical electrostatic boundary value problem has been formulated for the potential distribution in each of the regions (1 and 2). The solutions of differential equations for the first and second domains was obtained in the form:

$$V_1 = -4\pi e\sigma_0 P|x|, \quad (2)$$

$$V_2 = V_+ e^{\lambda x} + V_- e^{-\lambda x} + V_0, \quad (3)$$

where σ_0 is the surface charge density of the polymer layer, V_+ and V_- are the magnitudes of the potentials determined by the boundary conditions of regions 1 and 2, respectively, V_0 are the integration constants, λ is a parameter inversely proportional to the length of the Thomas–Fermi shielding.

In this study, we try to generalize previous results by considering a contribution to the total capacitance $C_{\text{tot}}^{-1} = C_q^{-1} + C^{-1}$ from quantum capacitance C_q , which arises as one of the electrostatic boundary conditions and modifies I–V measured characteristics. Indeed, in work [16] the authors modelled the interionic interactions in a slit-like pore by introducing a finite quantum capacitance C_q and observed its effect on the electrostatic interactions between ions. The induced surface charge is a function of the electric potential on the polymer layer surface $V_s(r)$ [16]:

$$\sigma(V_s(r)) \approx -\frac{\varepsilon}{4\pi} C_q V_s(r), \quad (4)$$

where $C_q = 4\pi e^2 n'(\mu)/\varepsilon$ is the linear quantum capacitance, n is the density of charge carriers, $\mu > 0$ ($\mu < 0$) is the chemical potential for electron (hole) doping. ($C_q = \infty$ for ideal metallic walls and is also voltage-depending).

The electrostatic potential V_1 must satisfy Poisson equation inside region 1

$$\vec{\nabla} \left(\varepsilon \vec{\nabla} V_1(\vec{r}) \right) = -\rho(\vec{r}), \quad (5)$$

where $\rho(\vec{r})$ is total charge density and ε is the dielectric constant of the material. In region 2, the potential V_2 satisfies

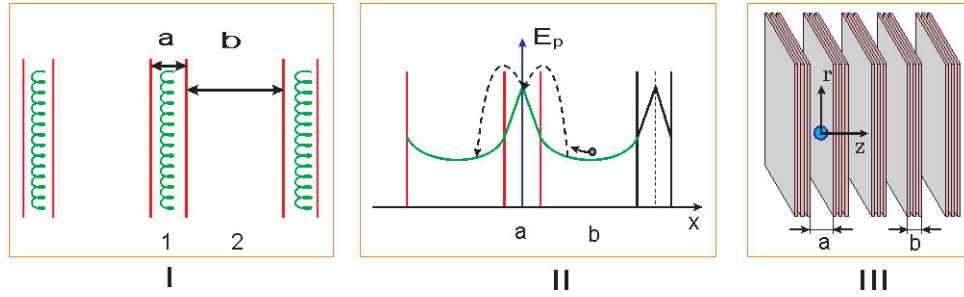


Fig. 6. Sketch of the InSe<PTHQ> nanostructure as N -sheets in the stack; the extended van der Waals (region 1) is of width a , and semiconductor layer (region 2) is of width b

Laplace's equation. Assuming the axis z is directed perpendicular to the plane of the region 1 and 2 (Fig. 6 (III)), the boundary value problem in such stack geometry can be written as

$$\frac{1}{r} \frac{\partial}{\partial r} \left(r \frac{\partial V_1}{\partial r} \right) + \frac{\partial^2 V_1}{\partial z^2} = -\frac{4\pi q}{\varepsilon} \frac{\delta_r(r)}{2\pi\sigma} \delta(z), \quad -\frac{a}{2} < z < \frac{a}{2}, \quad (6)$$

$$\frac{1}{r} \frac{\partial}{\partial r} \left(r \frac{\partial V_2}{\partial r} \right) + \frac{\partial^2 V_2}{\partial z^2} = 0, \quad -\frac{b}{2} < z < \frac{b}{2}, \quad (7)$$

where $\delta(z)$ is the 1D delta distribution function.

The boundary conditions for (6), (7) will obviously look like

$$\begin{aligned} V_2(r, \pm b) &= V_1(r, \pm a) = V_s(r), \\ \frac{\partial V_2}{\partial z}(r, \pm b) - \frac{\partial V_1}{\partial z}(r, \pm a) &= C_q V_s(r). \end{aligned} \quad (8)$$

Solutions of the boundary value problem (6), (7) with boundary conditions (8) for the first and second regions are, respectively:

$$\begin{aligned} V_1(r, z) &= -\frac{q}{\varepsilon} \int_0^{\infty} J_0(kr) \left(\text{sh}k|z| - \frac{(C_q + k)\text{sh}K + k\text{ch}K}{(C_q + k)\text{ch}K + k\text{sh}K} \cdot \text{ch}kz \right) dk, \\ V_2(r, z) &= \frac{q}{\varepsilon} \int_0^{\infty} \frac{ke^K J_0(kr) e^{-k|z|}}{(C_q + k)\text{ch}K + k\text{sh}K} dk, \end{aligned} \quad (9)$$

where $K = ka$ is dimensionless parameters (the separation between N layers in the stack are assumed to be the same and equal to a) and $J_0(kr)$ is the zeroth order Bessel function of the first kind.

Equation for $V_1(rz)$ shows that the electric potential, and thus the interionic interaction energy, decrease as the width a decrease. It is known that narrow pores with separations comparable to ion diameter are used in supercapacitors to minimize Coulombic repulsion between charges and thus maximize charge storage [17, 18]. To elucidate the mechanism of charge storage in narrow pores we have used an exactly solvable 1D lattice model where the interaction between N ions take place via nearest neighbor hopping [19]. We have calculated the density of the electronic states of the system with impurities in low

concentration and studied the localization effects in the considerable case of disordered 1D system where disorder is applied in form of randomly distributed realistic ions, leading to partly periodic Hamiltonian matrices. Our theoretical approaches for 1D lattice model of N ions, confined in slit-like pores, are completely corresponded to obtained experimental data and aforesaid consideration of Fig. 1.

The interaction energy between two ions, situated in the pore's midplane is written as

$$\beta U(R) = \frac{l_B}{a} \int_0^{\infty} J_0(KR) \frac{(\tilde{C}_q + K) \text{sh}K + K \text{ch}K}{(\tilde{C}_q + K) \text{ch}K + K \text{sh}K} dK, \quad (10)$$

where $K = kaR = r/a$, $\tilde{C}_q = C_q a$, $\beta = 1/(k_B T)$. Analysis of equation (10) shows that with the quantum capacitance increasing the interaction energy between two ions is screened and decreases by its absolute value.

The tunneling current for the InSe<PTHQ> nanostructure can be recorded as:

$$J_{eT} = e\gamma \sum_{\vec{p}} |T_{\vec{p}}|^2 \left(f^{(1)}(\vec{p}, \tilde{V}_1) - f^{(2)}(\vec{p}, \tilde{V}_2) \right), \quad (11)$$

where $T_{\vec{p}}$ is the transition matrix, $f^{(1)}(\vec{p}, \tilde{V}_1)$, $f^{(2)}(\vec{p}, \tilde{V}_2)$ are the distribution functions, respectively, in the first and second regions, \tilde{V}_1 and \tilde{V}_2 are modified by the external electric field potentials, \vec{p} is quasi-momentum, γ is the parametric constant. Distribution functions $f^{(1)}(\vec{p}, \tilde{V}_1)$, $f^{(2)}(\vec{p}, \tilde{V}_2)$ can be represented in the quasi-classical approximation. If the transition matrix $T_{\vec{p}}$ does not depend on the value of the applied external voltage U , then the tunneling current formula has the form

$$\begin{aligned} J_{eT} &= e\gamma S n_0 \left(e^{\frac{e\tilde{V}_1}{kT}} - e^{\frac{e\tilde{V}_2}{kT}} \right) e^{-\frac{U}{T}} \\ &= e\gamma S n_0 e^{\frac{e\tilde{V}_1}{kT}} \left(1 - e^{-\frac{U}{T}} \right), \end{aligned} \quad (12)$$

where the numerical value of S is equal to

$$\sum_{\vec{p}} |T_{\vec{p}}|^2 \exp\left(\frac{-\hbar^2 p^2}{2m^* kT}\right) \quad (13)$$

(m^* is effective mass). The last formula allows us to calculate the I-V curves in a wide region of bias voltage showing that

with increasing voltage U of the exponent can become much less than 1, which will correspond to the nature of the I - V characteristics in Fig. 5.

Although constructed N -barrier model neglects many aspects of energy storage in heterostructures and its predictions may not be easily verified in experiments due to complexity of real hierarchical structures, it allows to make analytical progress and further generalization which accounts for more complex phenomena. Indeed, in order to investigate the current-voltage characteristics in the constant magnetic field in the direction perpendicular to stack of nanosheets the average current density in each domain was represented in [20] in terms of Green's functions. The influence of the magnetic field causes both a reduction of the conductivity associated with delocalized charge carriers and a growth of the hopping conductivity, as well as the quantization of energy levels of charge carriers, in particular in impurity sub-bands, which can result in the oscillatory behavior of the real component of the impedance in the low-frequency interval.

To investigate this phenomenon in more detail, the complex impedance of the intercalated nanostructure $\text{InSe}\langle\text{PTHQ}\rangle$ was measured depending on the magnitude of the applied constant electric field. Thus, Fig. 7 shows the frequency dependences of the real part of the complex resistance on the magnitude of the applied constant electric field.

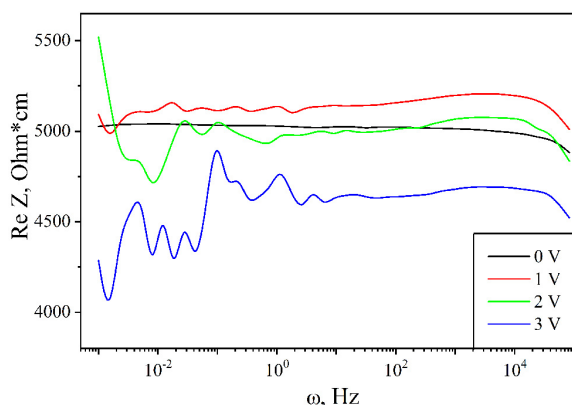


Fig. 7. Frequency dependences of the resistivity for the nanostructure $\text{InSe}\langle\text{PTHQ}\rangle$ at the corresponding values of the bias voltage

The constant electric field leads to the deformation of the low-frequency region $\text{Re} Z(\omega)$, and with increasing field magnitude, the deformation also increases sharply. This behavior indicates the presence of trap centers that capture and hold current carriers for a time associated with the half-cycle of the sinusoidal measuring signal. This can lead to the unusualness of the complex impedance, which will be manifested primarily in the transition to inductive behavior in the low-frequency region of the spectrum.

The Nyquist diagrams shown in Fig. 8 is a clear confirmation of aforesaid. The phenomenon of negative capacitance is well known, but there is currently no clear explanation. It is most often associated with the process of capture of injected carriers and their retention by the centers of adhesion for a time commensurate with the half-life of the sinusoidal signal [21, 22].

According to the second, more general mechanism, inductive behavior occurs even when the charge is introduced into layers of small or ultra-small size, i.e., the range of several nanometers [23].

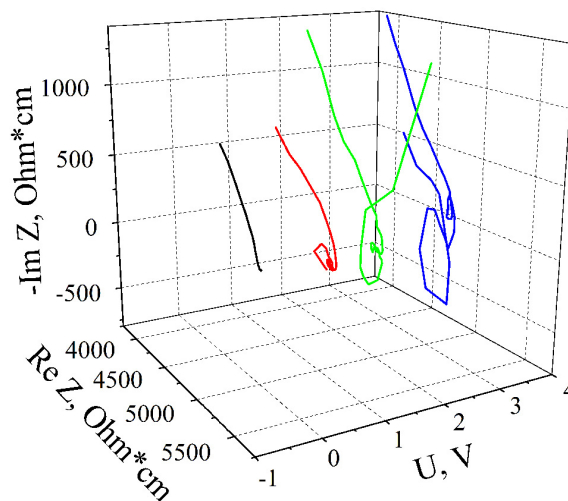


Fig. 8. Nyquist diagrams for the $\text{InSe}\langle\text{PTHQ}\rangle$ at the corresponding values of the bias voltage

As a result, an equivalent electric circuit the constructed impedance hodograph in accordance with Voigt's approach [13] will contain a series connection of two parallel $R||CPE$ links ($CPE_M||R_M$, $CPE_H||R_H$) and the third "inductive" link $L-CPE_{M\phi}||R_{M\phi}$, as shown in Fig. 9. Each of the links reflects the processes of charge transfer through the matrix material, the molecular polymer layer and their interfacial boundary, respectively. It contains an element of the constant phase of the CPE, the impedance of which in the complex plane is expressed as

$$Z_{CPE} = K^{-1}(j\omega)^{-\gamma}. \quad (14)$$

Here K is coefficient of proportionality; γ is a power indicator denoting the phase deviation, which reflects the distribution of capacity for each relaxation process.

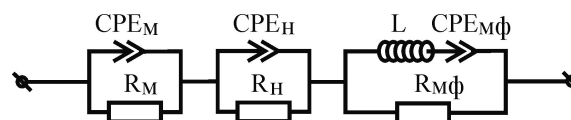


Fig. 9. A equivalent electric circuit for the nanostructure $\text{InSe}\langle\text{PTHQ}\rangle$ in accordance with Fig. 8

Checking the adequacy of the constructed model of the experimental data package showed reliable results: the Kramers-Kronig coefficient did not exceed $3 \cdot 10^{-5}$, the difference frequency dependences of the first order were completely random. All this gives grounds to propose the following cooperative nature of "negative capacity" in the studied structures.

It consists in the injection of carriers into quantum wells, their capture and retention along with recharging of deep levels of the crystalline matrix of indium selenide, which causes the appearance of a negative arc of complex impedance [24, 25].

To detail the physical mechanisms of current flow in the synthesized nanostructure, the temperature-dependent impedance was analyzed. To detail the physical mechanisms of current flow in the synthesized nanostructure, the temperature-dependent impedance was analyzed. As can be seen from Fig. 10 and 11, low-frequency oscillations of $\text{Re } Z(\omega)$ begin to appear at 0°C . However, in contrast to the action of a constant electric field, the inductive response in Nyquist diagrams is not observed, which indicates a different nature of the observed phenomenon.

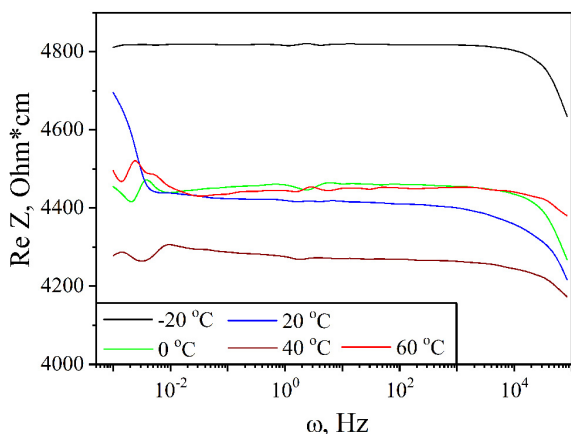


Fig. 10. Frequency dependences of the real part of the complex impedance for the nanostructure InSe<PTHQ> at different temperatures

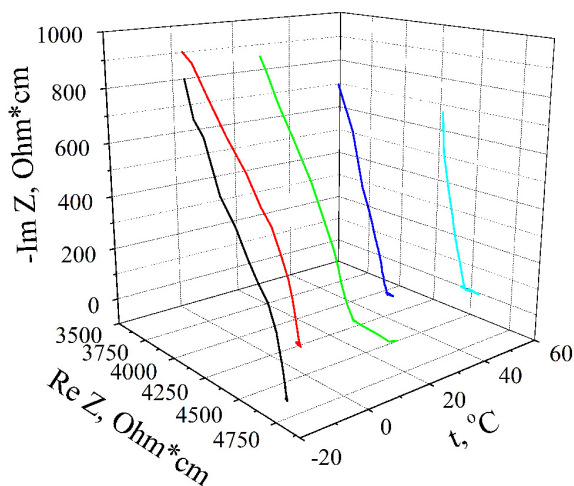


Fig. 11. Nyquist diagrams are constructed for the InSe<PTHQ> direction at different temperatures

Therefore, we can assume that in this temperature range only delocalized current carriers from energy levels near the Fermi level, the activation energy of which is proportional to room temperature, take part in the conductivity. This assumption is confirmed by the appearance of oscillations in the lowest frequency region starting from 0°C and above. This phenomenon indicates the emergence of a certain asymmetry of the density of states above and below the Fermi level in the specified temperature range.

The measured currents of thermally stimulated depolarization serve as a vivid confirmation of the above-mentioned mechanisms of electrical conductivity and energy structure of this nanostructure (Fig. 12).

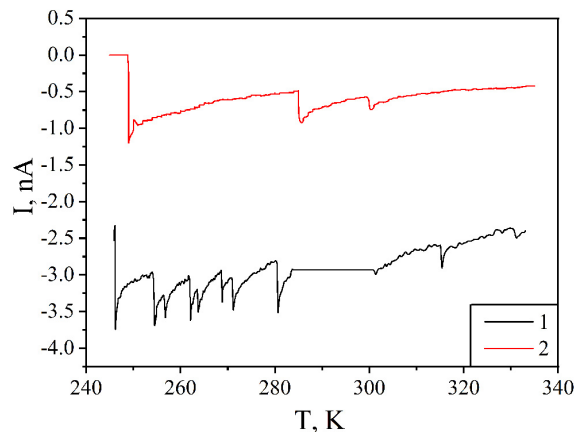


Fig. 12. TSD currents were measured for the original extended InSe matrix and InSe nano hybrid <PTHQ>

As we can see in both cases there is a relaxation of the homocharge, and the spectrum is transformed from a striped to a broadband with a high density of states.

4. CONCLUSIONS

For the first time, an inorganic/organic hybrid InSe<PTHQ> with 2-fold expansion of the crystal matrix was synthesized. As a result of the expansion of the single crystal, an N -stage ordered structure is formed. It consists of identical packets with slightly compressed interlayer distances compared to the original single crystal, which are separated by an extended area.

The oscillating behavior of the low-frequency region $\text{Re } Z(\omega)$ allows us to represent the synthesized nanostructure InSe<PTHQ> as an N -barrier structure with energy relief, in which the “stepwise” quantum wells are the result of distortion of energy levels at the interfacial boundaries. The processes of capture, retention, and release of current carriers from quantum wells are responsible for the inductive response.

The following effects were realized in the intercalated nano hybrid InSe<PTHQ>:

- photoinduced quantum capacity, which can be used in practice to convert and store solar energy at the quantum level;
- “negative capacitance” in the low frequency range, the magnitude of which can be controlled by the applied constant electric field. It can be used in electronics as nanoscale inductors controlled by an electric field.

REFERENCES

- [1] R. Schlesinger, F. Bianchi, and S. Blumstengel, C. Christodoulou, R. Ovsyannikov, B. Kobin, and N. Koch, “Efficient light emission from inorganic and organic semiconductor hybrid structures by energy-level tuning”, *Nat. Commun.*, vol. 6, no. 1, pp. 7754(1–7), Apr. 2015, doi: [10.1038/ncomms7754](https://doi.org/10.1038/ncomms7754).

- [2] W.-Q. Kan, J. Yang, Y.-Y. Liu, and J.-F. Ma, "Series of inorganic-organic hybrid materials constructed from octamolybdates and metal-organic frameworks: Syntheses, structures, and physical properties", *Inorg. Chem.*, vol. 51, no. 21, pp. 11266–11278, 2012, doi: [10.1021/ic300134z](https://doi.org/10.1021/ic300134z).
- [3] L. Dobrzycki and K. Woźniak, "1D vs 2D crystal architecture of hybrid inorganic-organic structures with benzidine dication", *J. Mol. Struct.*, vol. 921, no. 1–3, pp. 18–33, Dec. 2009, doi: [10.1016/j.molstruc.2008.12.027](https://doi.org/10.1016/j.molstruc.2008.12.027).
- [4] P. Chabecki *et al.*, "Functional energy accumulation, photo- and magnetosensitive hybridity in the GaSe-based hierarchical structures", *Energies*, vol. 13, no. 17, pp. 4321(1–16), Aug. 2020, doi: [10.3390/en13174321](https://doi.org/10.3390/en13174321).
- [5] F. Ivashchyshyn, A. Pidluzhna, D. Calus, O. Hryhorchak, P. Chabecki, and O. Makarchuk, "Multivoltaic GaSe clathrate as new hybrid functional nanostructure", *Bull. Pol. Acad. Sci. Tech. Sci.*, vol. 69, no. 2, pp. e136726(1–5), 2021, doi: [10.24425/bpasts.2021.136726](https://doi.org/10.24425/bpasts.2021.136726).
- [6] I. Grygorchak *et al.*, "Thermogalvanic and local field effects in SiO₂<SmCl₃> structure", *Appl. Nanosci.*, vol. 10, no. 12, pp. 4725–4731, May. 2020, doi: [10.1007/s13204-020-01447-2](https://doi.org/10.1007/s13204-020-01447-2).
- [7] M. Büttiker, Y. Imry, R. Landauer, and S. Pinhas, "Generalized many-channel conductance formula with application to small rings", *Phys. Rev. B.*, vol. 31, no. 10, pp. 6207–6215, May. 1985, doi: [10.1103/PhysRevB.31.6207](https://doi.org/10.1103/PhysRevB.31.6207).
- [8] G.V. Baryshnikov, R.L. Galagan, L.P. Shepetun, V.A. Litvin, and B.F. Minaev, "Synthesis and spectroscopic characterization of a new (aryl-SCN)_n polymer: Polythiocyanatohydroquinone", *J. Mol. Struct.*, vol. 1096, pp. 15–20, Apr. 2015, doi: [10.1016/j.molstruc.2015.04.040](https://doi.org/10.1016/j.molstruc.2015.04.040).
- [9] I.I. Grygorchak, "Intercalation: achievements, problems, outlook (Review)", *Phys. Chem. Solid State*, vol. 2, no. 1, pp. 7–57, 2001.
- [10] I. Dupliak *et al.*, "Influence of optical radiation and magnetic field on the properties of InSe clathrate", *Ukr. J. Phys. Opt.*, vol. 21, no. 3, pp. 115–125, 2020, doi: [10.3116/16091833/21/3/115/2020](https://doi.org/10.3116/16091833/21/3/115/2020).
- [11] F. Ivashchyshyn, I. Grygorchak, T. Gordiyuk, R. Shvets, and Y. Kulyk, "Effect of lattice expansion degree on properties and electromagnetic field response of InSe, GaSe and clathrates on their basis", *East. Eur. J. Enterp. Technol.*, vol. 6, no. 11, pp. 48–56, 2015, doi: [10.15587/1729-4061.2015.56576](https://doi.org/10.15587/1729-4061.2015.56576).
- [12] S. Luryi, "Quantum capacitance devices", *Appl. Phys. Lett.*, vol. 52, no. 6, pp. 501–503, 1988.
- [13] Z. Stoinov, B. Grafov, B. Savvova-Stoinova, and V. Yelkin, *Electrochemical Impedance*, Nauka, Moscow, 1991, [in Russian].
- [14] *Impedance spectroscopy. Theory, experiment and application*, eds. E. Barsoukov and J.R. Macdonald, Wiley interscience, Hoboken, New Jersey, 2005.
- [15] F. Ivashchyshyn, I. Grygorchak, P. Stakhira, V. Cherpak, and M. Micov, "Nonorganic semiconductor Conductive polymer intercalate nanohybrids: Fabrication, properties, application", *Curr. Appl. Phys.*, vol. 12, pp. 160–165, May 2012, doi: [10.1016/j.cap.2011.05.032](https://doi.org/10.1016/j.cap.2011.05.032).
- [16] A. A. Lee, D. Vella, and A. Goriely, "Quantum capacitance modifies interionic interactions in semiconducting nanopores", *EPL (Europhys. Lett.)*, vol. 113, no. 3, pp. 38005(1–6), Mar. 2016, doi: [10.1209/0295-5075/113/38005](https://doi.org/10.1209/0295-5075/113/38005).
- [17] S. Kondrat and A. Kornyshev, "Superionic state in double-layer capacitors with nanoporous electrodes", *J. Phys.: Condens. Matter.*, vol. 23, pp. 2–10, 2010.
- [18] C. Rochester, A. Sartor, G. Pruessner, and A.A. Kornyshev, "One dimensional double layer. The effect of size asymmetry of cations and anions on charge-storage in ultranarrow nanopores – an Ising model theory", *Russ. J. Electrochem.*, vol. 53, no. 10, pp. 1165–1170, 2017.
- [19] M. Klapchuk and I. Grygorchak, "The effect of additional off-diagonal disorder of interionic interaction on charge-storage in sub-nanometer pores of supramolecular carbon supercapacitors", *Math. Model. Comput.*, vol. 5, no. 2, pp. 147–157, 2018, doi: [10.23939/mmc2018.02.147](https://doi.org/10.23939/mmc2018.02.147).
- [20] M. Klapchuk and F.O. Ivashchyshyn, "Giant magnetoresistance effect in InSe?β-CD?FeSO₄?clathrate", *Mathematical Modeling and Computing*, vol. 7, no. 2, pp. 322–333, 2020.
- [21] N.A. Penin, "Otricatel'naya emkost' v poluprovodnikovykh strukturakh", *FTP*, vol. 30, no. 4, pp. 626–634, 1996, [in Russian].
- [22] J. Bisquert, H. Randriamahazaka, and G. Garcia-Belmonte, "Inductive behaviour by charge-transfer and relaxation in solid-state electrochemistry", *Electrochim. Acta.*, vol. 51, no. 4, pp. 627–640, Jun. 2005, doi: [10.1016/j.electacta.2005.05.025](https://doi.org/10.1016/j.electacta.2005.05.025).
- [23] I. Mora-Seró *et al.*, "Implications of the negative capacitance observed at forward bias in nanocomposite and polycrystalline solar cells", *Nano Lett.*, vol. 6, no. 4, pp. 640–650, Jan. 2006, doi: [10.1021/nl052295q](https://doi.org/10.1021/nl052295q).
- [24] I.I. Grygorchak, F.O. Ivashchyshyn, M.V. Tokarchuk, N.T. Pokladok, and O.V. Viznovych, "Modification of properties of GaSe <β-cyclodextrin <FeSO₄>> clathrate by synthesis in superposed electric and light-wave fields", *J. Appl. Phys.*, vol. 121, pp. 185501(1–7), May. 2017, doi: [10.1063/1.4983097](https://doi.org/10.1063/1.4983097).
- [25] P. Kostrobij, I. Grygorchak, F. Ivashchyshyn, B. Markovych, O. Viznovych, and M. Tokarchuk, "Generalized electrodiffusion equation with fractality of space-time: Experiment and theory", *J. Phys. Chem. A*, vol. 122, no. 16, pp. 4099–4110, Apr. 2018, doi: [10.1021/acs.jpca.8b00188](https://doi.org/10.1021/acs.jpca.8b00188).